AC 1

We sincerely thank Guido Blöcher for his review. His comments were very useful and helped us to improve the quality of our manuscript. Please find below a point-by-point response to the general and specific comments (comments of the reviewer in black and our response in red, text changes appear in italic font) .

On behalf of all authors, Yours sincerely,

Maximilian Oskar Kottwitz

General comments:

The general focus of the paper is to present a correction factor for the cubic law in the R-S space. This by its own is of particular interest. In contrast, all simulations were performed with a pressure difference of 0.01 Pa and laminar flow conditions are assumed. This opens the question, are the correction factors the same (in R-S space) for other pressure gradients and therefore other flow velocities.

Laminar flow conditions are essential for using the Stokes equations instead of the Navier-Stokes equations and are valid for Reynolds numbers below unity (see Zimmermann & Bodvarsson, 1996). Above that, inertial forces start to introduce turbulences which further reduce overall flowrates. By choosing a constant pressure difference of 0.01 Pa, we ensured that the maximal resulting Reynolds numbers is below unity. In figure 1, we show the Reynolds number Re (computed by $Re = \frac{\rho \bar{v} \bar{a}}{\mu}$, with fluid density ρ, volume average velocity $\bar{v}$, mean aperture $\bar{a}$ and fluid viscosity μ) as function of mean aperture $\bar{a}$. As evident from the picture, the bulk of the simulations range from 10-3 to 10-8. Which means, for sub-millimeter apertures, the pressure gradient could be larger than 0.01 Pa without interfering with the unity threshold. For sub-centimeter apertures, we reach the unity threshold, so strictly speaking, this poses an upper limit for the applicability of the computed correction factors. For pressure differences lower than 0.01 Pa, we generally assume the correction factors to be valid. If fractures with larger apertures (e.g. cm range) are considered, the applied pressure gradients need to be reduced such that they fulfill the above-mentioned criteria of Reynolds numbers below unity. Yet, if laminar flow conditions exist, the proposed correction factors remain applicable.

Although, a non-dimensional fracture roughness quantification-scheme is acquired, the authors could indicate the dimensions of their simulations. This would help to understand at which scale the correction scheme is applicable. Values of length, height, mean aperture, etc. should be mentioned either as absolute or relative values.

We indicated a fixed physical voxel size of 0.1 mm. With a constant model resolution of 512*512*128 voxels, this results in a model size of 51.2*51.2*12.8 mm. Table 1 gives input metrics used to generate the synthetic fractures. The resulting range of mean apertures ($\bar{a}_{min} = 1.910 * 10^{-04}\ m; \bar{a}_{max} = 4.961 * 10^{-03}\ m$) as well as absolute permeability values ($k_{min} = 6.786{*}10^{-14}\ m^2; k_{max} = 7.940 * 10^{-07}\ m^2$) were inserted a new table (table 2) at page 9.

This comment is the most important one. As mentioned before the presented approach seems highly applicable. Unfortunately, the proof with real data is missing. It would be nice to use, e.g. laboratory measurements, to proof the presented approach. If no data are available, we could provide surface scans with a resolution of 50 μm and related fracture permeability measurements. Furthermore, aperture distribution, mean aperture, contact area are known. The authors could show how they determine the S-R-values and can subsequently compare the corrected permeability values with the measurements. (contact: Guido Blöcher, bloech@gfz-potsdam.de)

The validation of the proposed concept with real data is truly of high interest. In fact, we are already preparing follow-up studies targeting exactly this:
In one study, we validate the results of the numerical simulations by using 3D printed versions of some fracture realizations generated in this study and perform laboratory experiments to obtain their permeabilities to subsequently compare them to their numerical equivalents.
In another study, we test the performance of the proposed correction scheme to predict permeabilities of real fractures by utilizing CT-scans of those (partly obtained from www.digitalrocksportal.org and partly self-acquired – by now a total of 32 CT-scans). It also incorporates simple pre-processing advices to prepare the CT data for numerical simulations and the computation of the S-R-values, which we by default calculate from voxel datasets.
We genuinely appreciate the offer of providing data, especially the fracture permeability measurements are of high interest. However, to fully capture the statistics of a fracture's aperture field (specifically in terms of its correlation length and contact areas) we require volumetric (voxel-based) data, rather than separated scans of fracture surfaces. By that, we hope to reflect the true matching of the opposing fracture surfaces, which determines the correlation length of the aperture field. Furthermore, we computed the S-R-values from volumetric data.
We fully understand the request for a proof with real data, however we think that this is beyond the scope of this methodological study and we think that it is more appropriate to deliver this in future studies.

Specific comments:

P1L2: Replace "Yet" with "In contrast".

Incorporated suggest change at indicated location.

P1L9: Here a sentence regarding the dimension of the simulation (length, width, and aperture) should be added.

We changed the sentence at P1L10 to:
Each fracture consists of two random, 25cm^2 wide self-affine surfaces with prescribed roughness amplitude, scaling exponent, and correlation length, which are separated by varying distances (mean apertures in submillimeter range) to form fracture configurations that are broadly spread in the newly formed two-parameter space.

P3L75: What means: low Reynolds numbers and low-pressure gradients? The authors should provide ranges where the presented approach is applicable.

We changed the sentence at P3L75 to:
Assuming, that the flow is solely laminar (Reynolds numbers below unity according to Zimmermann and Bodvarsson, 1996), the fluid viscosity is constant and . . .

P3L81: What is effective fluid viscosity? μ is the dynamic fluid viscosity.

We simplified the sentence at p3L81 to:
. . . with the fluid's dynamics viscosity μ, . . .

Figure 2: The vertical axis has no axis label. It seems it indicates the aperture. Since the aperture is provided by the color code, a 2D image would be sufficient.

Technically, a 2D image would be sufficient as vertical axis and colorbar provide the same information. However, we choose the 3D representation to put emphasis on the effective surface area increase caused by a lower Hurst exponent for equal mean and standard deviations. In 2D, we had the impression that this was not as straightforward to see. On top of that, the necessary visual comparison of mean and standard deviation by the black solid and dashed lines could not be realized in 2D.
This is why we would rather keep the Figure as is, while changing the caption as follows:
Two aperture fields constructed from synthetic fractures. Both aperture fields are based on the same sets of random numbers with varying Hurst exponents H, which is a) 0.4 and b) 0.8. The two statistical parameters $\bar{a}$ and σ_a are indicated by black solid and dashed lines, respectively. Axis units are in mm, while the

vertical axis (indicating aperture) is exaggerated by a factor of two for clarity. Note that $\bar{a}$ and σ_a are identical for a) and b). Increasing height fluctuations at smaller scales, caused by a lower Hurst exponent results in a larger effective surface area S for fracture a) compared to b).

P6L126: Often ϕ indicates the porosity but not here. I suggest using another symbol than ϕ to indicate the correction factor.

We decided to change the symbol from ϕ to χ throughout the paper, as we agree that the use of ϕ can lead to confusion.

P6L128: For S = 1 and R = 0 we would mimic flow between parallel plates. For this situation, the correction factor should be one and the cubic law could validate the simulation. This validation was done but is somehow hidden in figure 5. The authors should emphasis that this simple check was performed.

We added the following sentence at P9L197:
Perfect hydraulic efficiencies ($\chi = 1$) were validated by flow simulations in parallel-plate fractures.

P6L135: Why a representation of the matrix is required? Only the fracture is simulated and the boundary condition is a non-slipping boundary. It is not clear why the complete matrix-fracture-system is considered.

Numerically, we don't discretize the matrix. We zero out the corresponding entries in the jacobian matrix to gain computation time. However, we ensure constant spatial extents for all simulations for the volume integration of the velocity, such that all permeabilities are normalized to the same fracture volume.

P6L136-138: The sentence seems to be incomplete and should be rewritten. Furthermore, the macroscopic flow direction (y-direction) should be mentioned.

We changed the sentence at P6L136-138 to:
Different pressures are applied on two opposing boundaries ($\Delta P = 0.01$ Pa for all models), while the remaining boundaries are set to no-slip. This fixes the principal direction of fluid movement (here it is in y-direction, e.g. Fig. 3).

P6L141: This is an integration of v_y over the total volume and not a volume integral. Since v_x and v_z should be small compared to v_y these quantities could be used to determine v ÌE.

For directional permeabilities, we are just interested in the v_y component for the applied boundary conditions (no-slip at boundaries next to pressure boundaries). Considering of v_x and v_z would only be important, if we open the no-slip

boundaries (e.g. apply a linear gradient between opposing fracture boundaries). We updated the sentence at P6L141:
After ensuring that the numerically converged solution is obtained (see appendix A in Eichheimer et al., 2019), the velocity component parallel to the principal flow direction is integrated over the volume to compute the volume average velocity $\bar{v}$ according to: ...

P6L144: The dynamic viscosity is denoted with η before it was μ.

We changed the viscosity notation to μ.

Table 1: The number of parameter combinations for group 1 is given to be 400. If I multiply the n_{g1} (4*4*4*5) it should be 360. Furthermore, the fracture configurations for group 1 should be 360*r_{g1}=7200 but only 6400 are mentioned in the table caption.

Apologies, we indeed forgot to update the total number of parameter combinations to 320 (4*4*4*5). This results in 6400 geometries and 12800 flow simulations.

P8L157: Again, values about the fracture aperture and the representation by the voxels is missing.

We expanded the sentence at P8L157 by:
... with a fixed physical voxel size of 0.1 mm, resulting in a model domain of 51.2 x 51.2 x 12.8 mm.

We added the following at P8L166:
..., yet they all remain fully percolating (resulting mean apertures range from 0.15 to 4.96 mm).

P8L173: 12800 flow simulations are mentioned assuming 6400 fracture configurations. If comment 12 is corrected or explained the authors should revise the number of flow simulations (14400).

See comment above.

P9L194: In case the authors decided for another symbol than ϕ, they should correct the symbol here.

See comment above. Symbol was also changed in Figure 5 and Figure 7.

Figure 5: The figure is fine in color mode but almost no difference between blue and red is visible in greyscale mode. Maybe, the color scheme can be adjusted.

We revised the figure with a grey-scale friendly and also sequential colorbar (see figure 2), which makes more sense than a diverging one. Colour descriptions in the figure caption are changed accordingly.

P13L240: Please add a space after closure.

We incorporated suggest change at indicated location.

Figure9: The mean error norm was obtained for the considered fractures and applied boundary conditions. The authors should discuss if this error norm changes for other flow regimes regarding Reynold number, flow velocity, pressure gradients, etc..

Increasing the pressure gradient results in higher flow velocities, ultimately leading to larger Reynolds numbers. As discussed above, the results are only valid, if the Reynolds number is below or equal to unity, i.e. laminar flow conditions are present, which is a fundamental assumption of using the Stokes equations. Quantifying errors in flow regimes other than laminar would require solving the full Navier-Stokes equations, which is beyond the scope of this study but poses an interesting challenge for future work.

AC 2

We sincerely thank the referee for reviewing this manuscript. His/her constructive and well-structured comments helped us to advance our manuscript. Please find below a point-by-point response to the referee comments (comments of the reviewer in black and our response in red, text changes appear in italic font)

On behalf of all authors, yours sincerely,
Maximilian Oskar Kottwitz

Main comments:

* Large closures and percolation analysis:
I don't think it makes much sense to investigate closures R much larger than 1. Indeed, the hypothesis of perfect plastic closure (overlapping regions just disappear) is not too bad for configurations in which a moderate proportion of the fracture plane is closed (i.e., for $R \leq 1$). But for larger closures one would expect the real geometry to be significantly different from that obtained with this crude approximation. It turns out that the results relative to the hydraulic efficiency are shown only for $R < 1$. The study of percolation, on the contrary, is only interesting for $R > 1$ since the percolation probability starts taking values strictly smaller than 1 precisely for these configurations of large closure ($R > 1$). This section is therefore, in my opinion, rather irrelevant. I would suggest to remove it.

The main purpose of the percolation analysis was to narrow down the parameter space for the presented generation-procedure of synthetic fracture models for the fluid-flow simulations. On top of that, we also wanted to know if there is a dependency of percolation and contact fraction on the effective surface area of the fractures. Since there was no notable dependence on S, one could have already excluded this from the paper, but since we use parts of the data for our conceptual model in figure 10, we initially decided to keep it.
We are fully aware that realistic geometries with configurations of $R > 1$ should differ significantly from the synthetic geometries we generated here, and we agree that adding the percolation analysis to the results section could be misleading due to the points you mentioned. We therefore now shift the figure to the description of the synthetic dataset (section 2.3), as it potentially shows closure behavior in a statistical manner. We clarified in the text that this approximation is rather crude for fractures with $R > 1$ but necessary to get an idea of the boundaries of the parameter space, which ultimately helped us to synthesize our conceptual model in the discussion.

This led to a few changes in the paper:
Section 3.1 was removed and parts of it were inserted into section 2.3. Further-

more, we exchanged the names of group 1 and 2 (group 2 are now the fluid flow geometries) to be chronologically consistent.

In addition, we added this line to address your comment:
Following this, we have chosen to limit the fracture geometries for the fluid flow simulations to configurations with $R \leq 1$ to (i) exclude non-percolation systems and (ii) limit the effect of the above-mentioned "melting" hypothesis, which intensifies with increasing R.

We also include a new table (table 2) on page 9, indicating the value ranges of mean aperture, standard deviation of aperture, contact fraction, R and S as well as effective permeability for all models in group 2, as this was also requested in by Reviewer 1.

* Figures 5 and 6, and the corresponding discussion (pages 10 and 11):
Instead of showing a plot that is interpolated from the raw data using a Matlab function whose principle is not explained and whose parameters are not given, I would suggest that the authors perform their own box-averaging to show local mean values of S as a function of S and R, but also that they also provide similar information for the fluctuations of the statistics, for example in terms of the standard deviations of values within various (R,S) ranges. Such a figure coud be added following the model of Figure 5, and would complement it.
In a way the information provided in Figure 6 contains this type of information, but in a less straightforward manner, and though the interpretation provided by the authors is correct, the choice of words matters. This is not about the "accuracy of the presented model", this results from the fact that the model corresponds to the average behavior of a population, and that fluctuations in hydraulic are found within the population. These fluctuations are all the larger as the correlation length is larger. The model may be very accurate for the average behavior (and probably is). And the authors could provide a model for the standard deviation around the mean behavior by fitting the data of the figure I am suggesting above.

Presenting experimental data with that amount of complexity is always non-trivial. We have chosen the open-source "gridfit" routine (using a smoothening factor of 4 and their default interpolation settings, i.e. Delaunay triangulation) because we already have been using it for a while due to its convenience and found that it was also used in a few other publications. However, we agree that this might seem unintuitive in comparison to using box-averaging and standard fitting routines, although it delivers comparable results. To be on the safe side, we performed the box-averaging on the raw data as suggested above to obtain local mean and standard deviations (see figure 1 and 2). Here, we have chosen the box-sizes such that they always contain 20 or more data points. If this condition does not hold, the boxes were left blank on the plot.
We could integrate the new plots with the box-averaged data into the paper or use the visually more appealing interpolated "gridfit" data as already present.

There, the fluctuations of the hydraulic efficiency are indicated by the black contour lines. We prefer using the original figure, as we find that it generally shows the trends of the data quite well and is easier to interpret as it combines the average behavior and the fluctuations.
We were not aware that a model for the standard deviation would be helpful using this kind of model – thank you for pointing it out. To deliver that, we used the box-averaged standard deviation data, took the center points of each non-empty box and assigned the corresponding value to perform standard surface fitting. We found that functions of the form $(a * exp(R) + b) * (c * tanh(S) + d)$ gave reasonable approximations of the hydraulic efficiency fluctuations, whereas the fitting parameters change for different correlation lengths. For that we generated a new table (table 3, page12), containing the fitting coefficients.

We changed the sentence on page 11, line 207 to:
To investigate the hydraulic efficiency fluctuations for similar fracture configurations, . . .

Add the end of the section, page 12 line 221, we added the following (note that we changed ϕ to χ throughout the text to prevent confusion with porosity - see RC1):
To quantify the hydraulic efficiency fluctuations (σ_χ) with respect to its correlation length, we provide a model of the form:
$\sigma_\chi = (a \times e^R + b)(c \times tanh(S) \ + \ d)$
with corresponding parameter values given by table 3.

Similarly I think that the wording used in the sentence of page 15, line 276, is misleading when mentioning "a prediction error of 26.7%.

We also changed the wording at 15, line 276 to:
The hydraulic efficiency as a function of effective surface area and fracture closure is given by eq. 16, its variability with respect to the correlation length is given by eq. 17 and table 3 whereas an overall numerical error of 7.2% *has to be considered.*

Accordingly, we had to change the abstract at page 1, line 20 to:
An equation was provided that predicts the average behavior of hydraulic efficiencies and respective fracture permeabilities as a function of their statistical properties. A model to capture fluctuations around that average behavior with respect to their correlation lengths has been proposed. Numerical inaccuracies were quantified with a resolution test, revealing an error of 7.2%.

*I am not quite sure I fully understand how the test on the accuracy of the numerical solution is done.

The numerical estimation of permeabilities is resolution dependent, i.e. it requires sufficient level of discretization to obtain the correct result. To investi-

gate the impact of this resolution dependency and subsequently the accuracy of the numerical solution at a certain level of discretization, proper resolution tests have to be conducted. In praxis, the same model is discretized with increasing resolutions and usually the resulting permeability converges to a constant value with respect to increasing resolutions – this is then thought to be the true solution. From this kind of calibration curves it is possible to estimate the numerical error at a certain level of discretization.
In our case, we first run simulations in several fractures with lc/L ratios of 1 at large resolutions and then subsequently reduce the resolution of the same models and investigate how the permeability fluctuates (quantified with the error norm in figure 8 as a function of voxel size, i.e 1/resolution).

Firstly, the notion of "uncorrelated part of a fracture" is strange to me, as the uncorrelated vs. correlated feature is a question of scale rather than location. Perhaps it is simply a question of formulation. Similarly, the sentence of line 228, "16 subsets are drawn that focus on the uncorrelated parts of the fractures that corresponds to ..." is not clear to me.

With "uncorrelated part of a fracture" we mean a smaller portion of the fracture where both fracture surfaces are fully uncorrelated. This can be any region of the fracture, with size equal to the correlation length, regardless of its location. The main surface features that inhibit flow are expressed in those regions, as above the correlation length the fracture is more or less planar. But since we simulated fractures of equal spatial extents with varying correlation lengths, we needed to quantify the numerical error caused by the loss of resolution in exactly those locations.
E.g: Our fractures are resolved with 512x512x128 voxels. For a fracture with lc/L of 1, the uncorrelated surface features are highly resolved with 512x512. In contrast to that, the uncorrelated regions of a fracture with lc/L of 1/16 are only resolved with a resolution of 32x32. The grey-dashed lines in figure 8 highlight the numerical error (7.2%) that is connected to the resolution we have chosen for our fractures with lc/L ratios of 1/16. For increasing lc/L ratios this error should reduce, as the uncorrelated regions become higher resolved.

In order to clarify this, we changed the wording on page 12, line 226 to:
As the most relevant roughness features are expressed within the uncorrelated region of a fracture (i.e., where $l_c = L$), ...

We also changed line 226-228 to:
For that, eight fractures with the size of $4096x4096x512$ *voxels and a* l_c/L *ratio of* $1/16$ *are generated in the same manner as explained in section 2.3. For each fracture, 16 subsets are drawn that focus uncorrelated regions of the fracture, resulting in subsets of* $256x256x512$ *voxels.*

* Last sentence of the paper: "This parametrization could easily be incorporated in a DFN modeling framework to investigate the hydraulic response at

reservoir scales".

Yes, it could. It could be interesting to substantiate, though, for two reasons.

First, this model is obtained for fractures of correlation length L/16. Does it still hold whatever the correlation length if it is smaller than L/16 ? If not the model could only be used in models of fractured reservoirs for which all fractures exhibit a ratio L/lc = 16.

Yes, you are right. Equation 17 can only be used for fractures in systems that are at least 16 times larger than the minimal correlation length. However, we can now use the model for the standard deviation of hydraulic efficiencies to incorporate fluctuations for systems that are closer to the correlation length. See comment below for changes in the paper.

Second, the hydraulic behavior of DFN of rough fractures is not necessarily properly described by that of a DFN of parallel plate fractures of suitably adjusted apertures. There can be coupling between fracture scale heterogeneity and network-scale heterogeneity, that is, fracture scale flow heterogeneity can in some cases modify the flow connectivity at the network scale. However de Dreuzy et al (JGR 2012) have shown that this can only occur if the correlation length is not significantly smaller than one or two tenths of the medium size. At reservoir scale this is clearly never the case. But this is not trivial and could be discussed.

Thank you for pointing that out. If DFN with spatial extents close to the fracture's correlation length are considered, fluctuations in the flow properties have to be taken into account. The paper you mentioned demonstrates nicely how this can be done.

We added the following sentence at page 16, line 293:
This parameterization can easily be incorporated in a DFN modeling framework to investigate the hydraulic responses at reservoir scales, assuming that the minimal correlation length is no longer than 1/16 *of the reservoir size. If DFN's of scales close to the correlation length are considered, fluctuations of the flow behaviour have to be taken into account (e.g., de Dreuzy et al., 2012), as this can modify network flow connectivity.*

Various comments on other points along the text:

* The introduction is rather short, but logically organized, and provides a proper summary of the state of the research on the topic so far. The authors use an approach relying on a large statistics of fracture with identical. They could mention that the first approach of this kind was proposed by Méheust and

Schmittbuhl in a JGR paper in 2001, studying populations of synthetic rough fractures with self-affine aperture fields (that is, for lc/L=1).

We changed page 3, lines 59 – 63 to:
Following Méheust and Schmittbuhl (2001,2003) the ratio between system size L, and the correlation length lc defines whether the fracture has an intrinsic permeability or not. Their statistical approach suggested that permeabilities of uncorrelated fractures (i.e., lc/L = 1) are strongly fluctuating and anisotropic for the same roughness configurations, revealing the importance of considering low lc/L ratios to be able to quantify an intrinsic fracture permeability.

* In the presentation of Eq. (1), the hypothesis of permanent flow is missing.

We changed page 3, line 76 to:
. . . , i.e., momentum balance (1) and continuity (2) equations, which for steady-state flow conditions are given in compact form by: ...

* In Eq. (6), the mathematical notation is strange: a is used both for the aperture field prior to negative values being put to 0, and for the the aperture field whose negative values have been put to 0. Of course when coding one may use the same variable name, overwriting the previous variable a, but mathematically they are two different quantities.

Of course, thanks for pointing out.
We changed the notation from $a(x, y)$ to $a_0(x, y)$ on page 4, lines 94 and 95 (eq. 6), page 5, lines 110 (eq. 9) and page 5, line 122.

* Page 5, line 104: "leaving H as a measure for the intensity of small scale roughness".

This explanation is a bit caricatural. H is rather a measure of the ratio between larger scale roughness and smaller scale roughness (the ratio being always larger than 1 since h¿0, but all the smaller as H is smaller).

You are right, this might sound over simplified.
We changed page 5, line 104 to:
. . . , leaving H as a measure for the ratio of large scale versus small scale roughness intensity.

* Equation (8): some authors choose to divide the standard deviation of the aperture by the mechanical aperture, which is the mean aperture prior to putting negative apertures to 0 and thus corresponds to the distance between the mean planes of the facing topographies. Is there a particular reason why you chose to use the mean aperture?

The reason for that is, that we wanted to have a parameter, that could be

computed from in-situ fracture data (e.g. CT-scans). There, it is very difficult to acquire information of the individual fracture surfaces, as one can only compute it from the entire void space. Also, we think that it better reflects effective properties of a fracture, as for fractures with large closures there might be trapped pore space within the fracture (we shortly addressed this on page 8, line 160).

* Page 4, line 113: why don't you express the condition of contact in terms of R ($R \geq 1/(3/\sqrt{2})$?

Thanks for pointing it out. In that context, it is better to express it in terms of R, rather than mean aperture.
We changed page 5 line 113 to:
... and the surfaces are in contact if $R \geq (3\sqrt{2})^{-1}$ *(see Brown, 1987).*

* Page 5, line 121: It seems that a simple way of presenting S would be as the ratio of the fracture surface's area to twice that of its projection on the fracture plane.

Yes, exactly. This is what is shown with the term $\frac{sa_f}{sa_c}$ in equation 10. However, you still have to normalize by the contact fraction.

We simplified the text on page 5 line 121 according to your suggestion:
For that, we calculate the ratio of the surface area of the fracture sa_f *to twice the area of its projection on the fracture plane (i.e., two times the base area perpendicular to the flow direction)* sa_c *and normalize it with the fractional amount of the aperture field that has opened, i.e. ...*

* Page 6: was the conservation of the total volumetric flow rate tested ? What are the relative flow rate fluctuations between all sections transverse to the mean flow ?

We understand the concern of the reviewer, that the numerical solution procedure might introduce errors in the mass conservation. In this case the result would be fluctuations in the relative flow-rate transverse to the principal flow direction. While computing the divergence of the continuity equation (eq. 2), we make sure, that the absolute mass-conservation residual is reduced down to 10^{-8}. Visualizing the spatial distribution of the mass-conservation residual (see figure 3 for an example) demonstrates this. Additionally, in Appendix A of Eichheimer et al., 2019 (https://doi.org/10.5194/se-10-1717-2019) it has been demonstrated that relative residual reductions lower than 10^{-7} deliver constant permeability values (using the same numerical code). Based on this, we conclude that the obtained solutions are sufficiently correct.

* Table 1: It would be interesting to have the mininum and maximum values

of R in the table.

See comment above, we inserted a new table on page 9 containing that information.

* Page 8, line 184-185, about the inset plot: the contact fraction is only controlled by the PDF of apertures prior to setting negative values to 0; that PDF is mostly independent of lc/L (though if one looks closely one may find a slight dependence), and therefore only dependent on the fracture closure. This is well known.

We agree. Because of that, we shifted the percolation analysis to the description of the synthetic dataset, rather than presenting it as new results (see comment above). However, we now know that this also holds for the way we compute the mean aperture (setting negative values to zero and then computing the PDF).

* Page 12, line 225: Here you probably mean "perpendicular to the fracture plane", i.e., the vertical direction if the fracture is horizontal.

In that case, the result of both expressions is the same. By applying pressure boundary conditions on two opposing fracture walls while setting the remaining to no-slip, we enforce a principal flow direction which in that case is parallel to the fracture plane. For porous media, however, this is not the case which is why we decided to keep the expression as is, but refining page 12, line 225 by:
. . . , the resolution perpendicular to the principal flow direction is the most crucial part.

* Equation (8): in this equation, it seems that the norm is simply the absolute value of the relative error. Why use a square inside a root mean square ?

Yes, you're right – thanks for pointing out.
We changed the notation of equation 18 to:
$||\delta_k|| = \left|\frac{k_r - k_{max}}{k_{max}}\right|$

* Discussion of page 14: here you could mention that the lower the value of l_c/L, the larger the impact of the vertical flow tortuosity on the fracture's permeability.

We changed page 14, lines 251-253 to:
Considering flow predictions for uncorrelated fractures (i.e. $l_c/L \geq 1$) is problematic. Blocked pathways connected to the early appearance of the percolation limit (see Fig. 4) or flow enhancing configurations ($\chi > 1$) as also observed by Méheust and Schmittbuhl (2000) are producing substantial variations in their hydraulic efficiencies. With decreasing lc/L ratios, the impact of vertical flow tortuosity on its permeability increases due to a larger portion of flow inhibiting

configurations compared to flow enhancing ones (see Méheust and Schmittbuhl, 2000). On the contrary, the fluctuations in the average flow behavior decrease significantly with decreasing lc/L ratios.

* Page 15, line 262: "correlation lengths that are equal to the size of the fracture .... seem rather unrealistic".

The origin of the correlation length is not generally known, is it ? Is it mechanical ? A fresh fracture without shift along the fracture plane would present a constant aperture field, one with a shift of length l would have a correlation length lc = l in that direction, but then the aperture field would be anisotropic.

We agree that little is known about the origin of the correlation length, but we follow the hypothesis of Brown, 1995, that it originates from mechanical principles. We simply wanted to make the point that a full fracture with a correlation length equal to the size of the fracture is unrealistic. If we considering the study of Schultz et al., 2008 (DOI: https://doi.org/10.1016/j.jsg.2008.08.001), the displacement of joints (d) scales with its length (L) by: $d = \alpha L^{0.5}$ with α-values in the order of 0.01 to 0.001. Assuming that the correlation length scales with the fractures displacement, results in maximal correlation-length-to-fracture-size ratios of 0.01. So it is not possible to have fractures with correlation length that is equal to their size. This highlights the need for further research on that topic.
To elaborate this in the paper, we changed page 14, lines 261-264 to:
From a mechanical perspective, correlation lengths that are equal to the size of the fracture seem rather unrealistic, considering that the shear displacement ds of fractures scales with their length Lf according to $ds = \alpha Lf^{0.5}$ *(Schultz et al., 2008). Using* α *values between 0.01 and 0.001, which is about the range for Moros joints in Schultz et al. (2008), results in a maximal lc/Lf ratio of ratio of 0.01. This thus illustrates that further research on fractures correlation lengths is required because the presence of it is omnipresent in most relevant studies ...*

* Page 15, line 269: Here and elsewhere I would use "parallel plate equivalent" (which refers to the geometry) rather than "cubic law equivalent", which involves a hydraulic concept. The two fractures are equivalent in that their mean apertures are identical (a geometric feature), not in that their hydraulic behavior is the same (this equality defines the fracture's hydraulic aperture).

Indeed, using the term "cubic law equivalent" could be misleading. We changed it throughout the paper to your suggestion at page 5, line 113 and line 119, page 6, line 123, page 9, line 195 and 196 and page 15, line 269.

Writing:

* Shouldn't the vectorial quantities (including nabla) appear in bold fonts?

We are not sure about that and would leave the final decision to the editor.

* Page 4, line 100: I would call the "rescaling factor" simply a "prefactor".

We incorporated the suggested change at page 4, line 100.

* Page 6, line 137: ")" should be removed after "0.01 Pa".

This was already changed in RC1.

* Page 6, line 145: here I'd write "with *eta* the fluid's dynamics viscosity".

We incorporated the suggested change at page 6, line 145. We changed the symbol for viscosity to μ to be consistent (This was already mentioned in the RC1).

* Page 8, line 176: I think "build" should be "built" here; please check.

Yes, correct. We corrected it at page 8, line 176.

* Page 12, line 219: "multiplied by" rather than "on".

We incorporated the suggested correction at page 12, line 219.

* Page 12, line 225: "the resolution perpendicular to the flow direction".

See comment above, we changed Page 12, line 225 to:
. . . , the resolution perpendicular to the principal flow direction is the most crucial part.

The hydraulic efficiency of single fractures: Correcting the cubic law parameterization for self-affine surface roughness and fracture closure

Maximilian O. Kottwitz[1], Anton A. Popov[1], Tobias S. Baumann[1], and Boris J. P. Kaus[1]

[1]Johannes Gutenberg University, Institute of Geosciences, Johann-Joachim-Becher-Weg 21, 55128 Mainz, Germany

Correspondence: Maxmilian O. Kottwitz (mkottwi@uni-mainz.de)

Abstract. Quantifying the hydraulic properties of single fractures is a fundamental requirement to understand fluid flow in fractured reservoirs. For an ideal planar fracture, the effective flow is proportional to the cube of the fracture aperture. ~~Yet~~In contrast, real fractures are rarely planar, and correcting the cubic law in terms of fracture roughness has therefore been a subject of numerous studies in the past. Several empirical relationships between hydraulic and mechanical aperture have been proposed, based up on statistical variations of the aperture field. However, often they exhibit non-unique solutions, attributed to the geometrical variety of naturally occurring fractures.

In this study, a non-dimensional fracture roughness quantification-scheme is acquired, opposing effective surface area against relative fracture closure. This is used to capture deviations from the cubic law as a function of quantified fracture roughness, here termed hydraulic efficiencies. For that, we combine existing methods to generate synthetic 3D fracture voxel models. Each fracture consists of two random, $25cm^2$ wide self-affine surfaces with prescribed roughness amplitude, scaling exponent, and correlation length, which are separated by varying distances to form fracture configurations that are broadly spread in the newly formed two-parameter space (mean apertures in submillimeter range).

First, we performed a percolation analysis on 600'000 synthetic fractures to narrow down the parameter space on which to conduct fluid flow simulations. This revealed that the fractional amount of contact and the percolation probability solely depends on the relative fracture closure.

Next, Stokes flow calculations are performed, using a 3D finite differences code on 6400 fracture models to compute directional permeabilities. The deviations from the cubic law prediction and their statistical variability for equal roughness configurations were quantified. The resulting 2D solution fields reveal decreasing cubic-law accordance's down to 1 % for extreme roughness configurations. We show that the non-uniqueness of the results significantly reduces if the correlation length of the aperture field is much smaller than the spatial extent of the fracture. ~~Under this assumption, an~~ An equation was provided that predicts the average behaviour of hydraulic efficiencies and respective fracture permeabilities ~~with a mean error of 26.7 %~~as a function of their statistical properties. A model to capture fluctuations around that average behaviour with respect to their correlation lengths has been proposed. Numerical inaccuracies were quantified with a resolution test, ~~adding another~~ revealing an error of 7 %~~on top of the previous one~~.

By this, we propose a revised parameterization for the permeability of rough single fractures, which takes numerical inaccura-

cies of the flow calculations into account. We show that this approach is more accurate, compared to existing formulations. It can be employed to estimate the permeability of fractures if a measure of fracture roughness is available, and it can readily be incorporated in discrete fracture network modeling approaches.

1 Introduction

The geometrical inhomogeneities of single fractures and their effect on fluid flow remains a crucial parameter for understanding the hydraulic properties of fractured reservoirs, such as crystalline or tight carbonate rocks with nearly impermeable matrices. Hence, it has wide-ranging industrial applicability in the fields of petroleum and gas production, geothermal energy recovery, CO_2 sequestration, nuclear waste disposal, and groundwater management. Fluid flow in fractured reservoirs is commonly modeled by the discrete-fracture-network (DFN) approach (Bogdanov et al., 2003; Klimczak et al., 2010; Leung et al., 2012; de Dreuzy et al., 2012), which relies on knowing the permeability of single fractures. The permeability of a single fracture is often approximated by the well known cubic law (Snow, 1969; Witherspoon et al., 1980), assuming that a fracture is composed of two parallel plates separated by a constant aperture. However, natural fracture walls show deviations from planarity, i.e., roughness, resulting in varying apertures within the fracture plane. On top of that, fluid-rock interactions like dissolution (Durham et al., 2001), erosion (Pyrak-Nolte and Nolte, 2016) and mineral growth (Kling et al., 2017) as well as the surrounding stress field (Zimmerman and Main, 2004; Azizmohammadi and Matthäi, 2017) further modify the geometry of a fracture, causing deviations of the parallel plate assumption.

Considerable effort has been made to study the effect of fracture surface roughness on flow and reactive transport behavior. Early attempts (Patir and Cheng, 1978; Brown, 1987; Zimmerman and Bodvarsson, 1996; Oron and Berkowitz, 1998) employed the 2D Reynolds equation, a simplification of the Navier-Stokes equations, which assumes that the cubic law holds locally with the aperture varying in the $x-y$ along-fracture plane. They derived semi-empirical functions that describe the deviations from the cubic law in terms of the mean and standard deviation of the aperture field. Increasing computational power led to numerical improvements, with 3D Lattice Boltzmann (Jin et al., 2017; Foroughi et al., 2018) or Navier-Stokes (Mourzenko et al., 1995; Brush and Thomson, 2003) simulations revealing the non-uniqueness of previous functional approximations of fracture permeability. Factors such as shear displacement (Kluge et al., 2017), tortuosity, and the degree of mismatch between the opposing fracture surfaces (Mourzenko et al., 2018) were demonstrated to affect fluid flow paths and permeabilities. Detailed analyses of exposed fracture surfaces have shown that self-affine fractal models are capable of quantifying surface roughness properties from thin-section- to outcrop-scale. Thereby, the dependence of surface roughness as a function of observation scale is captured by their scaling exponent (the so-called Hurst exponent H). For example, mode I fractures in a porous sandstone showed H of $0.4-0.5$ (Boffa et al., 1998; Ponson et al., 2007). Micro-fractures in Pomeranian shale featured H of 0.3 and 0.5 (Pluymakers et al., 2017), depending on the opening mode. In other studies, H of fault surfaces (mode II fractures) tends to fall in the range of $0.6-0.8$ with respect to slip orientation (Power and Tullis, 1991; Schmittbuhl et al., 1995; Bouchaud, 1997; Renard et al., 2006; Candela et al., 2012), regardless of rock type. Based on this, it is commonly assumed that a fracture consists of two opposing self-affine surfaces, and the resulting aperture field follows the same scaling relationship,

assuming both surfaces are uncorrelated (Plouraboué et al., 1995). However, observations of opposing fracture walls (Brown, 1995) have demonstrated that the two surfaces tend to be well correlated above a specific length scale and non-correlated below it, which poses an upper limit to the self-affine scaling in nature. ~~According to Méheust and Schmittbuhl (2003)~~Following Méheust and Schmittbuhl (2001, 2003), the ratio between system size L, and the correlation length l_c defines whether the fracture has an intrinsic permeability or not. Their statistical approach suggested that permeabilities of uncorrelated fractures (i.e., $l_c/L = 1$) are strongly fluctuating and anisotropic for the same roughness configurations, revealing the importance of considering low l_c/L ratios to be able to quantify an intrinsic fracture permeability.

Although extensively studied, no clear mathematical relationship between fracture roughness and permeability has been derived so far, leaving the cubic law as standardized parameterization in DFN modeling approaches. Thus, an applicable refinement is desired to promote their realism to help better understanding fluid flow on a reservoir scale. In this paper, existing algorithms are used to generate a large dataset of synthetic fractures covering all possible kinds of roughness configurations. Single-phase 3D Stokes flow calculations are then performed with a finite difference code, utilizing a high-performance-computing (HPC) cluster to handle the associated computational effort. By interpreting the statistical variations of the results, a refined parameterization of single fracture permeability is proposed, which is demonstrated to provide accurate predictions for the permeability of rough fractures.

2 Method & Data

2.1 Fluid flow in self-affine fractures

Generally, the flow of an incompressible Newtonian fluid is most accurately described by the Navier-Stokes equations (NSE). Assuming, that the flow is solely laminar ~~(low Reynolds number and low-pressure gradient)~~(Reynolds numbers below unity according to Zi , the fluid viscosity is constant and gravity is negligible at the system size, they reduce to the simpler Stokes equations, i.e., momentum balance (1) and continuity (2) equations, which for steady-state flow conditions are given in compact form ~~are given~~ by:

$$\mu \nabla^2 v = \nabla P, \tag{1}$$

$$\nabla \cdot v = 0, \tag{2}$$

with the ~~effective fluid~~fluid's dynamic viscosity μ, pressure P and velocity vector $v = (v_x, v_y, v_z)$, ∇, $\nabla\cdot$, and ∇^2 denote the gradient, divergence, and Laplace operator for 3D Cartesian coordinates, respectively.

These equations can be solved analytically for an idealized fracture, consisting of two parallel plates, vertically separated by a constant aperture a. Volumetric integration of the horizontally extended Poiseuille-flow solution yields the well known cubic law:

$$Q = -\frac{w a^3 \Delta P}{12 \mu}, \tag{3}$$

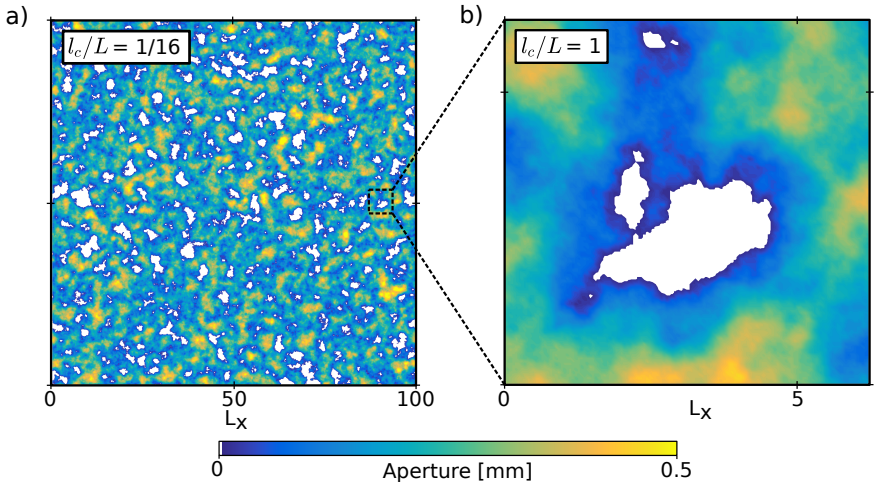

Figure 1. a) Aperture field of a synthetically generated fracture ($d = 1\ mm$, $\sigma_s = 0.5\ mm$, $H = 0.9$) with a l_c/L ratio of $1/16$. b) Zoom-in showing the uncorrelated part of the aperture field. Units of L_x are in mm.

with total volumetric flow rate Q, fracture width w and pressure gradient along the fracture ΔP (see Zimmerman and Bodvarsson (1996) for a more detailed derivation). Combining equation 3 with Darcy's law for flow through porous media:

$$Q = -\frac{kA\Delta P}{\mu}, \tag{4}$$

with cross-sectional area A, leaves the intrinsic permeability k of an idealized fracture proportional to its aperture by $k \propto a^2/12$. For a rough walled fracture, the aperture is no longer constant but rather varying across the fracture plane. The mean planes of an upper and lower rough surface $s_u(x,y)$ and $s_l(x,y)$ are separated by a constant distance d to form $a(x,y)$ according to:

$$a(x,y) = \left[s_u(x,y) + \frac{d}{2}\right] - \left[s_l(x,y) - \frac{d}{2}\right]. \tag{5}$$

Depending on d, the surfaces may overlap at certain points and form contact areas, such that ~~$a(x,y)$~~ $a_0(x,y)$ is zero at these locations:

$$a_0(x,y) = \begin{cases} a & \text{if } a(x,y) > 0 \\ 0 & \text{if } a(x,y) \leq 0. \end{cases} \tag{6}$$

Assuming, that s_u and s_l are self-affine, the standard deviation σ of the aperture field computed at system size l scales as (Brown, 1995; Schmittbuhl et al., 1995):

$$\sigma = \begin{cases} \beta l^H & \text{if } 0 \leq l \leq l_c \\ \beta l_c^H & \text{if } l_c \leq l \leq L, \end{cases} \tag{7}$$

with the maximal system size L and the correlation length l_c. Below l_c, the fracture is uncorrelated, and it is well correlated above it (see Fig. 1 for a visual explanation). The ~~rescaling factor~~ prefactor β delivers information about the overall amplitude

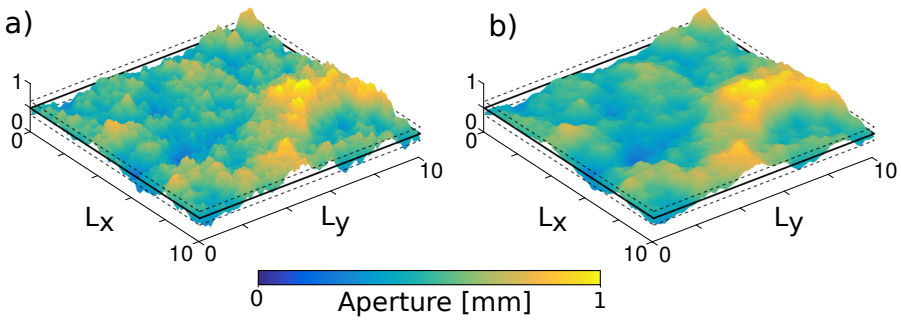

Figure 2. Two aperture fields constructed from synthetic fractures. Both aperture fields are based on the same sets of random numbers ~~and input parameters, such that the only~~ with varying ~~input parameter is the~~ Hurst ~~exponent~~ exponents H, which is a) 0.4 and b) 0.8. The two statistical parameters $\bar{a}$ and σ_a are indicated by black solid and dashed lines, respectively. ~~S of fracture a) is higher than S of b).~~ Axis units are in mm, while the vertical axis (indicating aperture) is exaggerated by a factor of two for clarity. Note that $\bar{a}$ and σ_a are identical for a) and b). Increasing height fluctuations at smaller scales, caused by a lower Hurst exponent results in a larger effective surface area S for fracture a) compared to b).

of the surface roughness. H typically denotes the scaling or Hurst exponent with $0 < H \leq 1$, whereas $H = 1$ corresponds to self-similar and $H < 1$ to self-affine scaling (e.g., Mandelbrot , 1982). Physically, self-affinity is expressed by higher height fluctuations at smaller scales, leaving H as a measure for the ~~intensity of~~ ratio of large scale versus small scale roughness intensity.

Here, we use the following two non-dimensional quantities to quantify the geometry of a rough fracture: (i) the relative closure R and (ii) the effective surface area S. We compute the relative closure by dividing the standard deviation of the aperture field at the maximal system size σ_a by the average aperture field $\bar{a}$:

$$R = \frac{\sigma_a}{\bar{a}}, \tag{8}$$

with $\bar{a}$ defined by:

$$\bar{a} = \frac{1}{L_x L_y} \int_{x=0}^{L_x} \int_{y=0}^{L_y} a_0(x,y)\,dx\,dy. \tag{9}$$

This quantity or its reciprocal is commonly used to infer the amount of contact between the opposing fracture walls (Patir and Cheng, 1978; Brown, 1987; Zimmerman and Bodvarsson, 1996; Méheust and Schmittbuhl, 2000). Theoretically, it falls in the range $0 < R \leq \infty$, whereas $R = 0$ shows perfect accordance with ~~the cubic law~~ parallel plates and the surfaces are in contact if ~~$\bar{a} \leq 3\sqrt{2}\sigma_a$~~ $R \geq (3\sqrt{2})^{-1}$ (see Brown, 1987).

Furthermore, one requires a parameter that quantifies the effective surface roughness of a fracture since fractures with different H can have equal R values (see Fig. 2 for a visualization of the non-uniqueness of R). We, therefore, introduce a new quantity,

the "effective surface area S". This parameter uniquely combines varying amplitudes and scaling exponents, because an increase in fracture surface area is the direct consequence of increasing roughness. For that, we calculate the ratio of the surface area of the fracture sa_f ~~is calculated, divided by the surface area of the cubic law equivalent with non-zero aperture~~ to twice the area of its projection on the fracture plane (i.e., two times the base area ~~of the system~~perpendicular to the flow direction) sa_c ~~, and normalized~~ and normalize it with the fractional amount of the aperture field that has opened, i.e.:

$$S = \left(\frac{sa_f}{sa_c}\right)\left(\frac{1}{1-c}\right), \tag{10}$$

with c being the contact fraction of the aperture field (i.e. where ~~$a(x,y) = 0$~~$a_0(x,y) = 0$), which leaves $1 \leq S \leq \infty$, with $S = 1$, showing perfect accordance with ~~the cubic law~~parallel plates. To finally quantify the influence of fracture roughness on its intrinsic permeability, the proportionality resulting from the cubic law needs to be corrected (e.g., Witherspoon et al., 1980) by applying a correction factor according to:

$$k \propto \phi\chi\frac{a^2}{12}. \tag{11}$$

The approximation of ~~ϕ~~ χ in terms of quantified fracture roughness, i.e. ~~$\phi(R,S)$~~$\chi(R,S)$, is the main subject of this study.

2.2 Numerical permeability estimation

To simulate the laminar flow of an incompressible, isothermal, and isoviscous fluid, we use a 3D binary voxel model input. We solve the linearized momentum balance (eq. 1) and continuity (eq. 2) equation in 3D, using velocity and pressure as primary variables. The coupled system is implemented in the open-source software package LaMEM (Kaus et al., 2016). LaMEM is a 3D staggered grid finite-difference code, which is based upon PETSc (Balay et al., 2018). The software is massively parallel

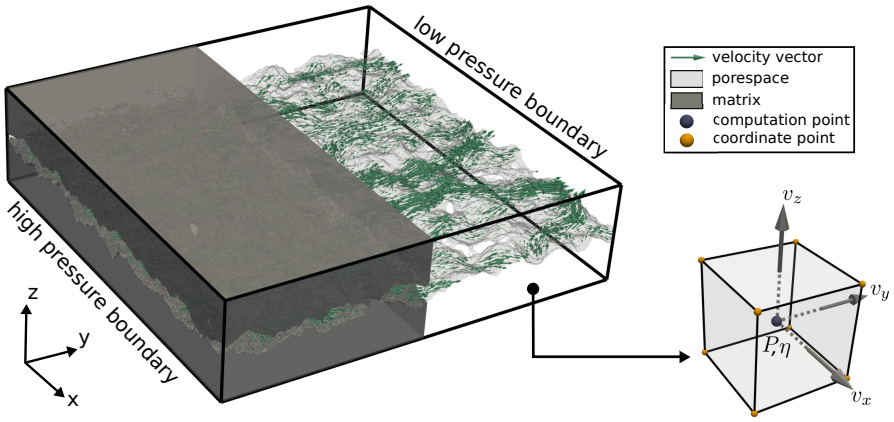

Figure 3. Model setup employed in the numerical simulations. The two boundaries where the pressure gradient is applied are indicated. The green velocity vectors are used for the computation of $\bar{v}$ and scaled according to their magnitude. The subfigure illustrates the staggered-grid discretization-scheme of a single voxel.

and thus optimized for the use of high-performance computing (HPC) clusters to enable the computation of high-resolution models in a reasonable amount of time. Here, the matrix is considered impermeable and constrained to no-flow conditions by forcing all three velocity components to be zero at the matrix-void-boundary. Besides, the staggered grid discretization scheme is rescaled at the fluid-matrix interface to provide higher accuracy (Eichheimer et al., 2019). ~~Two constant pressures~~ Different pressures are applied on two opposing boundaries ($\Delta P = 0.01$ Pa ~~)~~ for all models~~to provide the same pressure gradient)are applied on two opposing boundaries, fixing the direction of fluid movement with the two remaining boundaries~~), while the remaining boundaries are set to no-slip. This fixes the principal direction of fluid movement (here it is in y-direction, e.g. Fig. 3). After ensuring that the numerically converged solution is obtained (see appendix A in Eichheimer et al., 2019), the ~~volume integral of the velocity component oriented~~ velocity component parallel to the ~~flow direction $\bar{v}$ is computed as~~principal flow direction is integrated over the volume to compute the volume average velocity $\bar{v}$ according to:

$$\bar{v} = \frac{1}{V} \int_V |v_y| \, dy, \tag{12}$$

with the domain volume V. To finally obtain the intrinsic permeability k_i, $\bar{v}$ is substituted into Darcy's law for flow through porous media, similar to the approach of Osorno et al. (2015):

$$k_i = \frac{\eta \bar{v}}{\Delta P} \frac{\mu \bar{v}}{\Delta P}, \tag{13}$$

with the fluid~~dynamic viscosity η~~'s dynamic viscosity μ.

~~Model setup employed in the numerical simulations. The two boundaries where the pressure gradient is applied are indicated. The green velocity vectors are used for the computation of $\bar{v}$ and scaled according to their magnitude. The subfigure illustrates the staggered-grid discretization scheme of a single voxel.~~

2.3 Synthetic fracture dataset

As in-situ data of fractures are rarely accessible and limited to the size of drill cores, numerical studies commonly rely on a stochastic generation approach for synthetic fractures (e.g., Brown, 1995; Candela et al., 2010). Here, we numerically generate isotropic self-affine surfaces with a MATLAB script (Kanafi, 2016), which makes use of random theory and fractal modeling techniques (Persson et al., 2004). It uses the standard deviation of surface heights σ_s, the Hurst exponent H, the cutoff length l_c, and the system size L in x and y direction as input parameters to obtain $s_u(x, y)$ and $s_l(x, y)$, which are built from two independent Gaussian random number fields. The code is slightly modified, such that the seeds for the random number generator are prescribed to produce reproducible results. The mean planes ($x - y$ coordinate plane in both cases) of s_u and s_l are separated by varying values of d according to equation 5 to simulate different closure stages of the fracture. Since ignoring mechanical deformation is a common practice (Brown, 1987; Méheust and Schmittbuhl, 2000, 2003; Mourzenko et al., 2018), we also assume that both surfaces are in contact at the locations where they overlap. Finally, the data is transferred into a 3D voxel space of $512 \times 512 \times 128$ voxels with a fixed physical voxel size of 0.1 mm, resulting in a model domain of $51.2 \times 51.2 \times 12.8$ mm. The relative closure and the effective surface area are computed according to equations 8 and 10, respectively. It is important to note that both quantities are computed only within the effective pore space of the fracture parallel to the direction of

the applied pressure gradient because only this contributes to the overall flow. For some configurations, it might be possible to have small amounts of trapped pore space within the fracture, that must be excluded before further numerical treatment. We separate the datasets generated in this study into two groups~~. One is used for numerical flow simulations (group 1), the other for analyzing the percolation probabilities (group 2). Each group consists of several parameter combination sets with a~~ , each wich specific sets of input-parameter combinations and certain number of realizations (input values are listed in table 1). ~~We have chosen the values such that applicability to nature is ensured, and numerical stability is sustained for the flow simulations, as shown later . The fractures in group~~ The first group is used to analyze the percolation probabilities and determining the parameter boundaries for geometries of group 2, which are later used for for numerical flow simulations. To check, whether each fracture configuration in group 1 ~~are classified from "closed" to "open" joints according to Bieniawski (1989), yet they all remain fully percolating. This condition does not hold for the fracture models in group 2. They are solely generated to be used in a recursive flood-filling routine (e.g., Torbert, 2016), written in MATLAB to check whether the configuration can~~ is able to transmit fluids, i.e., if it is percolating or not~~. For the numerical fluid flow experiments in geometries of group 1, we implemented the following workflow: First~~, we apply a recursive flood-filling ~~algorithm on the initial 3D model along x-direction. R and S are calculated on the resulting effective pore space, followed by a numerical permeability estimation, as explained above, in the same direction~~MATLAB routine (e.g., Torbert, 2016). Then, ~~we rotate the initial model by 90° in the $x-y$ plane, and the procedure explained above is repeated. In this manner, two-directional permeability values for every fracture are obtained, resulting in a total sum of 12800 fluid-flow simulations.~~

3 ~~Results~~

2.1 ~~Percolation analysis~~

Table 1. ~~Synthetic fracture dataset details.~~ Minimal and maximal input values for parameters d, σ_s, H and l_c/L. n denotes the total number of increments, including minimum and maximum. Subscripts $g1$ and $g2$ indicate data for group 1 or 2, respectively. Thus, multiplying the n values of each parameter gives the total number of parameter combinations (~~400~~ 6000 for group 1, ~~6000~~ 320 for group 2). The number of realizations for a set (i.e. the number of different random number seeds used to generate the surfaces with one peculiar parameter combination) are given in the footnotes, resulting in a total of ~~6400 and~~ 600000 and 6400 fracture configurations for group 1 and 2, respectively.

Parameter	Dimension	$\min_{g1}$	$\max_{g1}$	n_{g1}	$\min_{g2}$	$\max_{g2}$	n_{g2}
d	mm	~~0.2 5 4~~ 0.01	1	20 ~~σ_s mm~~	0.2	~~0.5~~ 5	4
σ_s	mm	0.1	0.6	6	0.2	0.5	4
H	-	0.1	1.0	~~4~~ 10	0.1	1.0	~~10~~ 4
l_c/L	-	1/16	1	5	1/16	1	5

$r_{g1} = 100$, $r_{g2} = 20$

~~Percolation probability p (eq. 14) and the mean fractional amount of contact c as a function of relative closure R for all fracture realization sets of group 1 and 2. Different shades of blue indicate different l_c/L ratios as given in the legend, whereas black lines show best fits to the data.~~

~~The~~ the percolation probability p represents the mean value of n fracture realizations ~~build~~ built from one specific input parameter combination, such that:

$$p = \frac{1}{n}\sum_{i=1}^{n} p_i \,, \text{ with } p_i = \begin{cases} 1 \text{ if percolating} \\ 0 \text{ if non-percolating.} \end{cases} \tag{14}$$

Figure 4 shows the percolation probability as a function of relative closure R, as there was no notable variation with respect to their effective surface areas. ~~Note that R is computed for the effective pore space of a fracture, and there is none for non-percolating systems. Thus, the presented mean R values are computed only for percolating realizations within a parameter combination set. The completely non-percolating realization sets ($p = 0$) are excluded from the plot.~~ Generally, the percolation probability starts reducing from 1 at $R \approx 1$ and converges to zero at $R \approx 5$. Higher l_c/L ratios show earlier convergences to their percolation limit, as visible from the two fitted lines for l_c/L 1 and $1/16$. From the inset plot, it is evident that the contact fraction of all models only depends on the relative closure R, ~~with the best fit given by the following equation:~~

~~$c = \alpha^{tanh(R^{-0.6011} - 2.609) + 0.987}$,~~

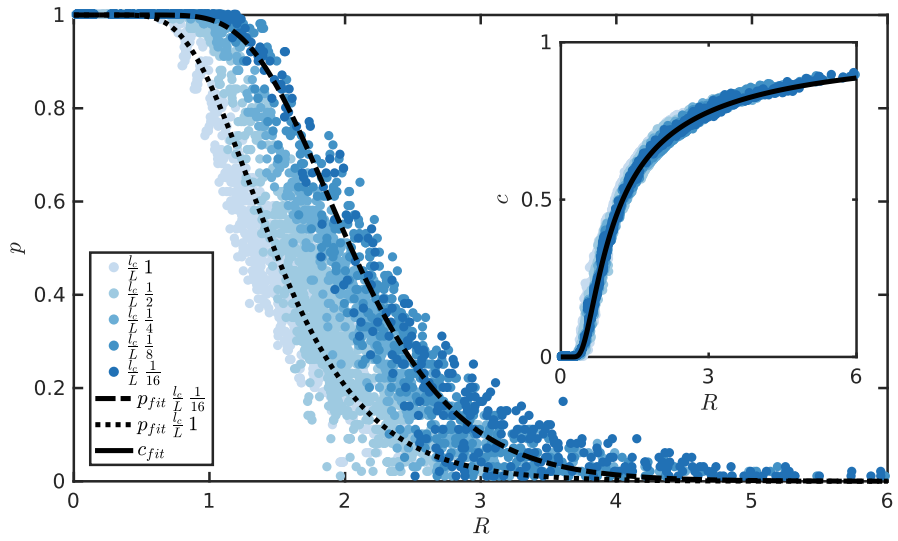

Figure 4. Percolation probability p (eq. 14) and the mean fractional amount of contact c as a function of relative closure R for all fracture realization sets of group 1 and 2. Different shades of blue indicate different l_c/L ratios as given in the legend, whereas black lines show best fits to the data.

Table 2. Resulting minimal and maximal values for mean aperture ($\bar{a}$), standard deviation of the aperture field (σ_a), contact fraction (c), relative fracture closure (R), effective surface area (S) and numerical fracture permeability (k_m) for the fracture geometries in group 2.

Parameter	$\bar{a}$	σ_a	c	R	S	k_m
Dimension	m	m	-	-	-	m^2
min	1.91×10^{-4}	1.16×10^{-4}	0	0.03	1.04	6.78×10^{-14}
max	4.96×10^{-3}	8.51×10^{-4}	0.44	0.99	2.49	7.94×10^{-7}

~~with $\alpha = 4.046 \cdot 10^{-7}$. The~~ first contact between both walls occurs ~~for $R \approx 0.23$~~at $R \geq 3\sqrt{2}\sigma_a$, which is in good accordance with Brown (1987). Following this, we have chosen to limit the fracture geometries for the fluid flow simulations to configurations with $R \leq 1$ to (i) exclude non-percolation systems and (ii) limit the effect of the above-mentioned "melting" hypothesis, which intensifies with increasing R. To ensure applicability to nature, the input values for group 2 (see table 1) are chosen, such that the resulting fracture geometries are classified from "closed" to "open" joints according to Bieniawski (1989) . The resulting parameter-ranges for fractures in group 2 can be found in table 2. For the numerical fluid flow simulations, we implemented the following workflow: First, we apply a flood-filling algorithm on the initial 3D model along x-direction. R and S are calculated on the resulting effective pore space, followed by a numerical permeability estimation, as explained above, in the same direction. Then, we rotate the initial model by 90° in the $x-y$ plane, and the procedure explained above is repeated. In this manner, two-directional permeability values for every fracture are obtained, resulting in a total sum of 12800 fluid-flow simulations.

3 Results

3.1 Hydraulic efficiency

In the following section, we present the results of the numerical fluid flow experiments within the geometries of group ~~1.~~ 2. For this, we normalize the numerically computed permeabilities (k_m) by the permeability predicted by the cubic law (k_{cl}) with equivalent mean aperture $\bar{a}$ of the associated effective pore space:

$$\phi\chi = \frac{k_m}{k_{cl}}. \tag{15}$$

Consequently, one can use the hydraulic efficiency ~~ϕ~~ χ as the correction factor in eq. 11 to apply the cubic law to rough fractures. In that way, a fracture whose configuration is close to the ~~ideal cubic law~~ parallel plates geometry shows excellent hydraulic efficiency with ~~ϕ~~ χ close to one. In the R-S-space, the ~~cubic law~~ parallel plate fracture configuration exclusively corresponds to a single point with coordinates $(0,1)$. Perfect hydraulic efficiencies ($\chi = 1$) were validated by flow simulations in parallel-plate fractures.

The key result of this study, a model that corrects the cubic law in terms of quantified fracture roughness, is proposed in Fig. 5. Due to the complexity of the results, we fitted a regularized surface with a MATLAB function called "gridfit" (DErrico,

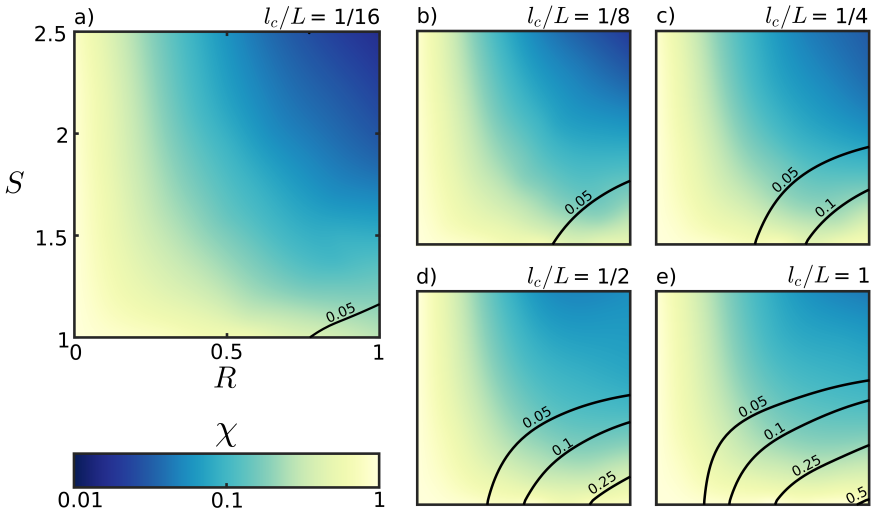

Figure 5. The distribution of the hydraulic efficiency ~~ϕ~~ χ for different l_c/L ratios as a function of R and S. Both axes limits in *a* correspond with *b*-*e*. ~~Red~~ Dark blue colour indicates poor hydraulic efficiency, whereas ~~blue~~ lighter colour shows increasing accordance with the cubic law. The black contour lines indicate the absolute residuals to the fitted surface (Compare with Fig. 6).

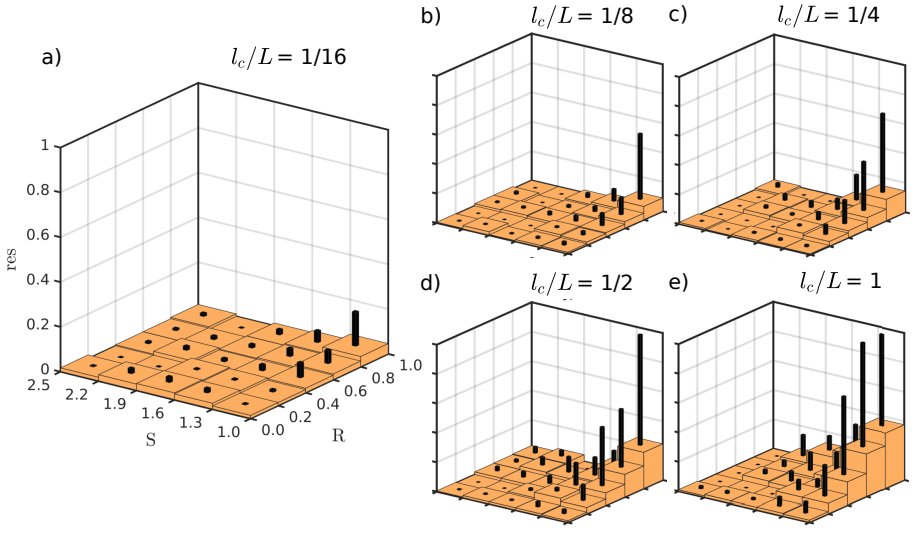

Figure 6. Absolute residual values of the fitted surfaces in Fig. 5 for different l_c/L ratios as a function of R and S, binned into equally sized boxes. All axes limits in *a* correspond to the ones in *b*-*e*. Orange boxes indicate the mean absolute residual value of the specific bin, whereas the smaller black boxes on top give the maximum absolute residual.

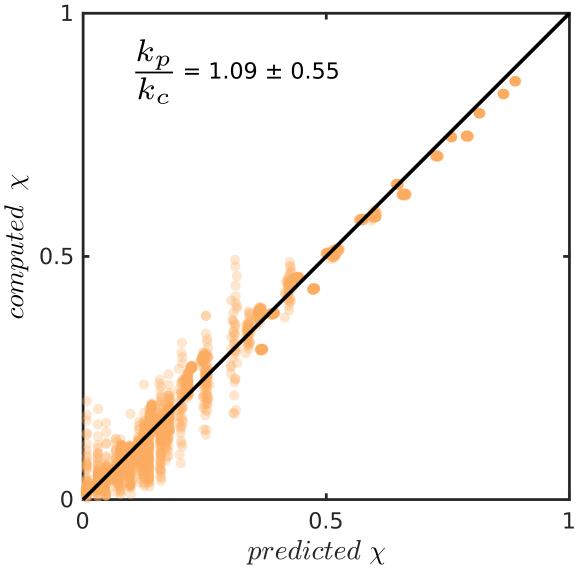

Figure 7. Parity plot of predicted versus computed hydraulic efficiency χ for a total of 2554 fractures with an l_c/L ratio of $1/16$. Black line indicates the location of perfect parity. Inlet data gives the mean and standard deviation of predicted (k_p) over computed (k_c) permeabilities that correspond to all data points in the plot.

2006) to approximate the solution in R-S space. The function can interpolate scattered data within a prescribed bounding box and a certain amount of smoothing, resulting in a clearer solution image compared to conventional interpolation techniques. Furthermore, to enable an adequate basis for the fitting, the data was cropped above $R = 1.0$ and $S = 2.5$ to provide sufficient data density in R-S-space, which reduces the total amount of simulations used for the fitting from 12800 to 10292.

The results display significant deviations from the cubic law approximation, even for fractures where both surfaces are not in contact (i.e., $R \leq 0.23$). We obtain the lowest ~~ϕ~~ χ values in regions of high R and S, with a general trend of increasing ~~ϕ~~ χ for larger l_c/L ratios.

To ~~estimate the accuracy of the presented model~~investigate the hydraulic efficiency fluctuations for similar fracture configurations, the absolute residuals of the fitted surface from Fig. 5 to the simulated data are computed. As before, we fit a regularized surface through the scattered points from which we extract the displayed contour lines (Fig. 5). They indicate that the goodness of the fit reduces with increasing l_c/L ratios, especially in the lower right corner. Hence, the non-uniqueness of the data reduces for lower l_c/L ratios, which can be even better seen in Fig. 6. A regional, maximum residual of about 0.2 for fractures with a l_c/L ratio of $1/16$ enables a more or less unique parametrization refinement, which is not the case for higher l_c/L ratios. Our finding that low l_c/L ratios show lower reduced variability is consistent with the results of Méheust and Schmittbuhl (2003).

An easy integration of this parametrization refinement into a DFN framework requires a mathematical approximation of the

Table 3. Resulting minimal and maximal values for mean aperture ($\bar{a}$), standard deviation of the aperture field (σ_a), contact fraction (c), relative fracture closure (R), effective surface area (S) and numerical fracture permeability (k_m) for the fracture geometries in group 2.

l_c/L	a	b	c	d
1/16	0.0428	0.1652	-0.8226	0.8822
1/8	0.6517	-0.3135	-0.6751	0.6625
1/4	0.9509	-0.7343	-0.7852	0.7672
1/2	1.0491	-0.9632	-1.2065	1.1752
1	1.3267	-1.3174	-1.6613	1.6178

fitted surface shown in Fig. 5 a), which was found by the following equation:

$$\phi\chi = 1 - (0.4809\tanh(0.5139S) + 0.5408)\tanh\left(\frac{R}{39.28\tanh(-2.451S) + 39.47}\right) \tag{16}$$

~~Parity plot of predicted versus computed hydraulic efficiency for a total of 2554 fractures with an l_c/L ratio of 1/16. Black line indicates the location of perfect parity. Inlet data gives the mean and standard deviation of predicted (k_p) over computed (k_c) permeabilities that correspond to all data points in the plot.~~ To predict single fracture permeability, it is only necessary to know the mean and standard deviation of the aperture field ($\bar{a}$ and σ_a), the fractional amount of surface contact (c) and the surface area protruding into the void space (sa_f). From these values, R and S are computed to infer the hydraulic efficiency ~~ϕ~~ χ with eq. 16, which is then multiplied ~~on~~ by the permeability predicted by the cubic law with aperture $\bar{a}$ (see eq. 11). Fig. 7 demonstrates the accuracy of eq. 16 to predict hydraulic efficiencies and accompanying permeabilities for fractures with l_c/L ratios of $1/16$. To quantify the hydraulic efficiency fluctuations (σ_χ) with respect to its correlation length, we provide a model of the form:

$$\sigma_\chi = (a \times e^R + b)(c \times tanh(S) + d) \tag{17}$$

with corresponding parameter values given by table 3.

3.2 Accuracy of the numerical solution

Numerical inaccuracies in solving the Stokes flow equations related to the resolution of the numerical models potentially have an important impact on the results shown here. For numerical permeability estimations (e.g., Osorno et al., 2015), the resolution perpendicular to the principal flow direction is the most crucial part. As the most relevant roughness features are expressed within the uncorrelated ~~part~~ region of a fracture (i.e., where $l_c = L$), it is necessary to examine the numerical error introduced due to resolution loss therein. For that, eight fractures with the size of ~~4096x4096x512 voxels~~ $4096 \times 4096 \times 512$ voxels and a l_c/L ratio of $1/16$ are generated in the same manner as explained in section 2.3. For each fracture, 16 subsets are drawn that focus ~~the uncorrelated parts of the fractures that corresponds to a l_c/L ratio of 1/16~~uncorrelated regions of the fracture, resulting in subsets of $256 \times 256 \times 512$ voxels. By this, the fracture part oriented perpendicular to the applied pressure gradient is over-resolved by a factor of two. The resolution of these initial models is then consecutively reduced

down to $16 \times 16 \times 32$ voxels (see inlay of Fig. 8 for a workflow sketch) while maintaining a constant dimensional aspect ratio. The resulting permeability at every stage (k_r) is then compared to the result at maximal resolution (k_{max}), assuming that this represents the most accurate solution. Finally, we compute the error norm according to:

$$||\delta_k|| = \sqrt{\left(\frac{k_r - k_{max}}{k_{max}}\right)^2} \left| \frac{k_r - k_{max}}{k_{max}} \right| \tag{18}$$

Ideally, the error norm should get negligible at the highest resolution. Fig. 8 shows the mean error norm of a total of 128 uncorrelated fracture subsets as a function of voxel size Δr. A mean error of about 0.01 % at maximal resolution indicates optimal convergence to the most accurate solution, which validates the numerical procedure. The voxel size of the numerical models used in this study ($0.1\ mm$) results in an acceptable mean error of 7.2 %, as indicated in Fig. 8.

4 Discussion

Many studies report that the cubic law increasingly deviates with increasing relative fracture closure (Patir and Cheng, 1978; Brown, 1987; Zimmerman and Bodvarsson, 1996), which is usually attributed to the flow channeling around the contact spots within the fracture, introducing an in-plane tortuosity that reduces the permeability. We quantified the deviations from the cubic

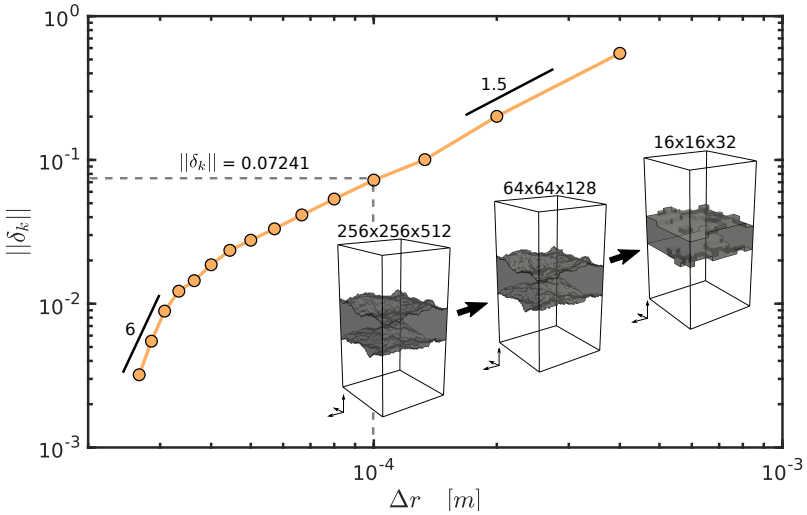

Figure 8. Error norm computed by eq. 18 as a function numerical voxel size Δr. The orange line depicts the mean error of 128 different fracture subsets discretized with decreasing resolutions. The figure inlay sketches the down-sampling procedure is sketched: The maximal resolution is consecutively decreased by 16 in horizontal and 32 voxels in vertical direction (displayed is the maximal, intermediate and minimal reduction stage). Dashed gray lines indicate the voxel size and associated error norm of the numerical simulations used to provide the refined single fracture permeability parameterization. Black lines highlight the convergence rate by showing local slopes as indicated by the attached values.

law due to vertical roughness features (i.e., amplitudes or Hurst exponents, see Fig. 5). The results suggest that with increasing fracture surface area protruding into the fluid phase, more drag force accumulates at the fluid-matrix interface, which resists the flow and leads to reduced permeabilities. It is not possible to capture these vertical variations in the flow field with previous 2D modeling approaches (e.g., Patir and Cheng, 1978; Brown, 1987; Renshaw, 1995; Zimmerman and Bodvarsson, 1996), which then results in a biased prediction and the need for more parameters to ensure an adequate quantification. Fig. 9 highlights this issue by computing the norm $||\delta_k||$ between measured and predicted permeabilities for all fractures in this study. With a mean error of 26.7 % eq. 16 delivers a better prediction compared to the mentioned studies.

As already shown by Méheust and Schmittbuhl (2003), the uncertainty for predicting fracture flow is a function of its l_c/L ratio. Considering ~~only the uncorrelated part of a fracture~~ flow predictions for uncorrelated fractures (i.e. $l_c/L \geq 1$) ~~for flow predictions~~ is problematic. Blocked pathways connected to the early appearance of the percolation limit (see Fig. 4) or flow enhancing configurations (~~$\phi > 1$~~$\chi \geq 1$) as also observed by Méheust and Schmittbuhl (2000) are producing substantial variations in their hydraulic efficiencies. With decreasing l_c/L ratios, the impact of vertical flow tortuosity on its permeability increases due to a larger portion of flow inhibiting configurations compared to flow enhancing ones (see Méheust and Schmittbuhl, 2000) . On the contrary, the fluctuations in the average flow behaviour decrease significantly with decreasing l_c/L ratios. This suggests that predicting hydraulic properties is constrained to fractures, whose sizes are significantly greater than their correlation lengths. Theoretically, the correlation length is mainly controlled by shear offset and respective gouge generation (Brown, 1995; Méheust and Schmittbuhl, 2000). With the assumption of a perfectly matched fracture ($l_c = 0$) at its nucleation stage, it is tempting to propose that most natural fractures actually meet the conditions of low l_c/L ratios and subsequently enable the

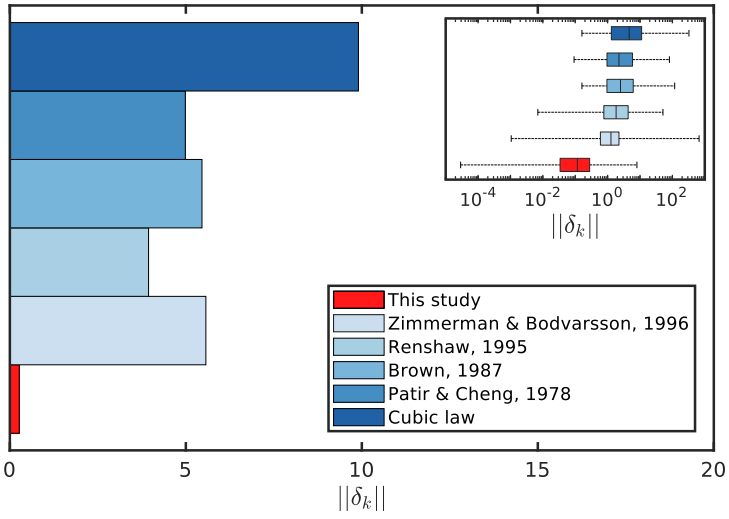

Figure 9. Mean error norm δ_k (see eq. 18) of all fractures considered in this study for different prediction models. The mean error norm recorded for this study is 0.267. Inlet plot shows box and whisker plots incorporating all outliers, i.e. representing minimum and maximum recorded values.

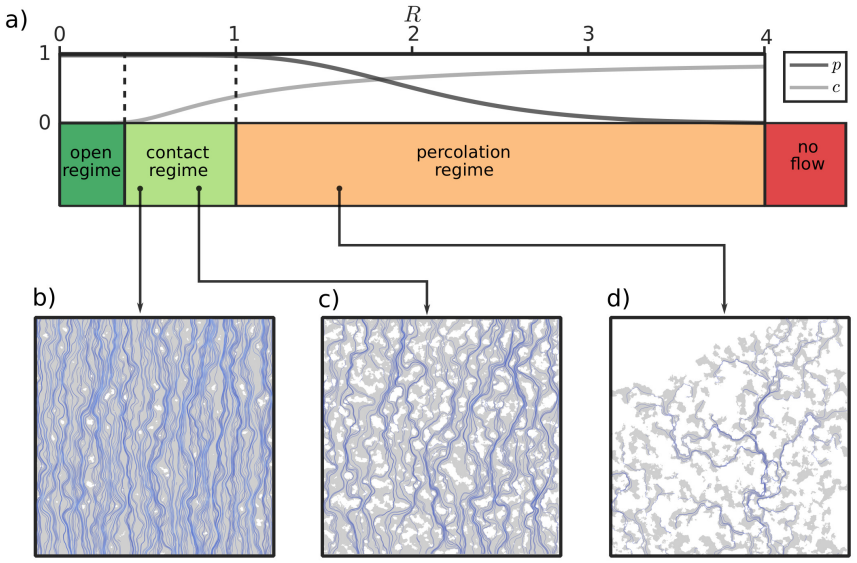

Figure 10. A sketch of the three different closure regimes, indicated as a function of R with corresponding p and c. The lower part of the figure shows three examples of fluid flow simulations from the indicated regimes. Grey shaded area is fracture void space, whereas white regions indicate contact between both surfaces. Blue lines depict chosen streamlines, approximated from the resulting Stokes velocity vectors.

prediction of their hydraulic properties. However, so far, little is known about naturally existing correlation lengths in fractures, as the imaging of in-situ fractures is limited to the size of drill cores. Only Brown (1995) report measurements of l_c by analyzing the power spectral densities of composite topographies for two matched profiles on opposing joint surfaces, shedding some light into their natural ranges. From a mechanical perspective, correlation lengths that are equal to the size of the fracture (i.e., l_c/L ratios close to 1) seem rather unrealistic, but further research considering that the shear displacement d_s of fractures scales with their length L_f according to $d_s = \alpha {L_f}^{0.5}$ (Schultz et al., 2008). Using α values between 0.01 and 0.001, which is about the range for Moros' joints in Schultz et al. (2008), results in a maximal l_c/L_f ratio of 0.01. All of that illustrates, that further research on fractures correlation lengths is required because the presence of correlation lengths in fractures it is omnipresent in most relevant studies (Brown, 1995; Mourzenko et al., 1996; Méheust and Schmittbuhl, 2003; de Dreuzy et al., 2012; Pyrak-Nolte and Nolte, 2016; Mourzenko et al., 2018).

5 Conclusions

To understand the effects of fracture surface roughness on fluid flow, we performed numerical simulations of high-resolution 3D Stokes-flow within fractures for a large synthetic dataset. By consolidating varying asperity amplitudes and roughness scaling within a new quantity, that accounts for the effective increase of surface roughness compared to its cubic law parallel

plate equivalent, we were able to provide a new way to characterize fracture roughness. By combining the effective surface area with the relative fracture closure, we established a two-parameter characterization scheme that reads similar to a phase diagram. It is utilized to quantify the hydraulic efficiency of single fractures empirically, i.e., the correction factor applied to the current state-of-the-art fracture permeability parametrization (cubic law). Our findings confirm the results of Méheust and Schmittbuhl (2003), and highlight that predicting fracture flow is constrained to scales of at least 16 times larger than the correlation length. ~~Under this assumption, the~~ The hydraulic efficiency as a function of effective surface area and fracture closure is given by eq. 16~~with a mean prediction error of 26.7 % and a~~ , its variability with respect to the correlation length is given by eq. 17 and table 3, whereas an overall numerical error of 7.2 % has to be considered. Ultimately, we used the percolation probability and contact fractions to classify three different closure regimes that differ in terms of their hydraulic interpretation:

(i) The open regime defines fractures whose surface walls are not in contact with each other (e.g., unconfined dilatant or karstified fractures). In this regime, we generally observe a good agreement of the cubic law with hydraulic efficiency between $70-100\%$ and only extreme roughness configurations (e.g., needle-shaped mineral coatings) result in larger deviations.

(ii) The contact regime is characterized by fractures exhibiting a rapidly decreasing hydraulic efficiency from $70-10\%$ up to $1\ \%$ in extreme cases, which is caused by strong three-dimensional channeling due to surface roughness and increasing fracture closure. Likely, this regime is most suitable for subsurface conditions, as a certain amount of contact between both fracture surfaces is required to withstand confining pressures.

(iii) The percolation regime incorporates fracture configurations that do not percolate at all due to blocked fluid pathways. Here, we do not incorporate fluid flow data, but it is plausible that the hydraulic efficiency is very poor with a maximum of 25%, which will quickly converge to 0% due to the effect of decreasing percolation probability with further closure. We observe the no-flow boundary at $R \approx 6$.

Our results generally help to understand the hydraulic response induced by different types of fracture geometries and refine the parametrization of single fracture permeability given by the cubic law. Moreover, the developed quantification scheme allows monitoring and parameterizing the hydraulic and geometric evolution of fractures during aperture field-shaping processes. This parameterization can easily be incorporated in a DFN modeling framework to investigate the hydraulic responses at reservoir scales, assuming that the minimal correlation length is no longer than $1/16$ of the reservoir size. If DFN's of scales close to the correlation length are considered, fluctuations of the flow behaviour have to be taken into account (e.g., de Dreuzy et al., 2012), as this can modify network flow connectivity.

Code availability. https://bitbucket.org/bkaus/lamem/src/master/ ; commit: 9c06e4077439b5492d49d03c27d3a1a5f9b65d32

Author contributions. MOK wrote the initial draft of the manuscript, performed numerical simulations, analyzed the data and generated the figures. AAP supervised and designed the study, provided the computational framework and edited the manuscript. TSB assisted to data fitting and edited the manuscript. BJPK helped designing the study, assisted to find an analytical model and edited the manuscript.

Competing interests. The authors declare that they have no competing interests

Acknowledgements. This work has been funded by the Federal Ministry of Education and Research (BMBF) program GEO:N, ~~PERMEA~~ ~~project~~grant no. 03G0865A. The authors gratefully acknowledge the computing time granted on the supercomputer Mogon II at Johannes Gutenberg University Mainz (hpc.uni-mainz.de).

References

Azizmohammadi, S. and Matthäi, S. K.: Is the permeability of naturally fractured rocks scale dependent?, Water Resources Research, 53, 8041–8063, 2017.

Balay, S., Abhyankar, S., Adams, M., Brown, J., Brune, P., Buschelman, K., Dalcin, L., Dener, A., Eijkhout, V., Gropp, W., et al.: PETSc Users Manual: Revision 3.10, Tech. rep., Argonne National Lab.(ANL), Argonne, IL (United States), 2018.

Bieniawski, Z. T.: Engineering rock mass classifications: a complete manual for engineers and geologists in mining, civil, and petroleum engineering, John Wiley & Sons, 1989.

Boffa, J. M., Allain, C., and Hulin, J. P.: Experimental analysis of fracture rugosity in granular and compact rocks, The European Physical Journal-Applied Physics, 2, 281–289, 1998.

Bogdanov, I. I., Mourzenko, V. V., Thovert, J.-F., and Adler, P. M.: Effective permeability of fractured porous media in steady state flow, Water Resources Research, 39, 2003.

Bouchaud, E.: Scaling properties of cracks, Journal of Physics: Condensed Matter, 9, 4319–4344, 1997.

Brown, S. R.: Fluid flow through rock joints: the effect of surface roughness, Journal of Geophysical Research: Solid Earth, 92, 1337–1347, 1987.

Brown, S. R.: Simple mathematical model of a rough fracture, Journal of Geophysical Research: Solid Earth, 100, 5941–5952, 1995.

Brush, D. J. and Thomson, N. R.: Fluid flow in synthetic rough-walled fractures: Navier-Stokes, Stokes, and local cubic law simulations, Water Resources Research, 39, 2003.

Candela, T., Renard, F., Bouchon, M., Brouste, A., Marsan, D., Schmittbuhl, J., and Voisin, C. (2009). Characterization of fault roughness at various scales: Implications of three-dimensional high resolution topography measurements. Mechanics, structure and evolution of fault zones, 1817–1851

Candela, T., Renard, F., Klinger, Y., Mair, K., Schmittbuhl, J., and Brodsky, E. E.: Roughness of fault surfaces over nine decades of length scales, Journal of Geophysical Research: Solid Earth, 117, 2012.

de Dreuzy, J.-R., Méheust, Y., and Pichot, G.: Influence of fracture scale heterogeneity on the flow properties of three-dimensional discrete fracture networks (DFN), Journal of Geophysical Research: Solid Earth, 117, 2012.

DErrico, J.: Surface Fitting using gridfit, MATLAB Central File Exchange, https://de.mathworks.com/matlabcentral/fileexchange/8998-surface-fitting-using-gridfit, 2006.

Durham, W. B., Bourcier, W. L., and Burton, E. A.: Direct observation of reactive flow in a single fracture, Water Resources Research, 37, 1–12, 2001.

Eichheimer, P., Thielmann, M., Popov, A., Golabek, G. J., Fujita, W., Kottwitz, M. O., and Kaus, B. J. P.: Pore-scale permeability prediction for Newtonian and non-Newtonian fluids, Solid Earth, 10, 1717–1731, https://www.solid-earth.net/10/1717/2019/, 2019.

Foroughi, S., Jamshidi, S., and Pishvaie, M. R.: New Correlative Models to Improve Prediction of Fracture Permeability and Inertial Resistance Coefficient, Transport in Porous Media, 121, 557–584, 2018.

Jin, Y., Dong, J., Zhang, X., Li, X., and Wu, Y.: Scale and size effects on fluid flow through self-affine rough fractures, International Journal of Heat and Mass Transfer, 105, 443–451, 2017.

Kanafi, M. M.: Surface generator: artificial randomly rough surfaces, MATLAB Central File Exchange, https://de.mathworks.com/matlabcentral/fileexchange/60817-surface-generator-artificial-randomly-rough-surfaces, 2016.

Kaus, B., Popov, A. A., Baumann, T., Pusok, A., Bauville, A., Fernandez, N., and Collignon, M.: Forward and inverse modelling of lithospheric deformation on geological timescales, in: Proceedings of NIC Symposium, http://hdl.handle.net/2128/9842, 2016.

Klimczak, C., Schultz, R. A., Parashar, R., and Reeves, D. M.: Cubic law with aperture-length correlation: implications for network scale fluid flow, Hydrogeology Journal, 18, 851–862, 2010.

Kling, T., Schwarz, J.-O., Wendler, F., Enzmann, F., and Blum, P.: Fracture flow due to hydrothermally induced quartz growth, Advances in Water Resources, 107, 93–107, 2017.

Kluge, C., Milsch, H., and Blöcher, G.: Permeability of displaced fractures, Energy Procedia, 125, 88–97, 2017.

Leung, C., Hoch, A., and Zimmerman, R.: Comparison of discrete fracture network and equivalent continuum simulations of fluid flow through two-dimensional fracture networks for the DECOVALEX–2011 project, Mineralogical Magazine, 76, 3179–3190, 2012.

Mandelbrot, Benoit B. The fractal geometry of nature. Vol. 173. New York: WH freeman, 1983.

Méheust, Y. and Schmittbuhl, J.: Flow enhancement of a rough fracture, Geophysical Research Letters, 27, 2989–2992, 2000.

Méheust, Y. and Schmittbuhl, J.: Geometrical heterogeneities and permeability anisotropy of rough fractures, Journal of Geophysical Research: Solid Earth, 106.B2, 2089–2102, 2001.

Méheust, Y. and Schmittbuhl, J.: Scale effects related to flow in rough fractures, Pure and Applied Geophysics, 160, 1023–1050, 2003.

Mourzenko, V. V., Thovert, J.-F., and Adler, P. M.: Permeability of a single fracture; validity of the Reynolds equation, Journal de Physique II, 5, 465–482, 1995.

Mourzenko, V. V., Thovert, J.-F., and Adler, P. M.: Geometry of simulated fractures, Physical Review E, 53, 5606, 1996.

Mourzenko, V. V., Thovert, J.-F., and Adler, P. M.: Conductivity and Transmissivity of a Single Fracture, Transport in Porous Media, 123, 235–256, 2018.

Oron, A. P. and Berkowitz, B.: Flow in rock fractures: The local cubic law assumption reexamined, Water Resources Research, 34, 2811–2825, 1998.

Osorno, M., Uribe, D., Ruiz, O. E., and Steeb, H.: Finite difference calculations of permeability in large domains in a wide porosity range, Archive of Applied Mechanics, 85, 1043–1054, 2015.

Patir, N. and Cheng, H.: An average flow model for determining effects of three-dimensional roughness on partial hydrodynamic lubrication, Journal of lubrication Technology, 100, 12–17, 1978.

Persson, B., Albohr, O., Tartaglino, U., Volokitin, A., and Tosatti, E.: On the nature of surface roughness with application to contact mechanics, sealing, rubber friction and adhesion, Journal of Physics: Condensed Matter, 17, R1–R62, 2004.

Plouraboué, F., Kurowski, P., Hulin, J.-P., Roux, S., and Schmittbuhl, J.: Aperture of rough cracks, Physical review E, 51, 1675–1685, 1995.

Pluymakers, A., Kobchenko, M., and Renard, F.: How microfracture roughness can be used to distinguish between exhumed cracks and in-situ flow paths in shales, Journal of Structural Geology, 94, 87 – 97, 2017.

Ponson, L., Auradou, H., Pessel, M., Lazarus, V., and Hulin, J.-P.: Failure mechanisms and surface roughness statistics of fractured Fontainebleau sandstone, Physical Review E, 76, 036 108, 2007.

Power, W. L. and Tullis, T. E.: Euclidean and fractal models for the description of rock surface roughness, Journal of Geophysical Research: Solid Earth, 96, 415–424, 1991.

Pyrak-Nolte, L. J. and Nolte, D. D.: Approaching a universal scaling relationship between fracture stiffness and fluid flow, Nature communications, 7, 10 663, 2016.

Renard, F., Voisin, C., Marsan, D., and Schmittbuhl, J.: High resolution 3D laser scanner measurements of a strike-slip fault quantify its morphological anisotropy at all scales, Geophysical Research Letters, 33, 2006.

Renshaw, C. E.: On the relationship between mechanical and hydraulic apertures in rough-walled fractures. Journal of Geophysical Research: Solid Earth, 100(B12), 24629-24636, 1995

Schmittbuhl, J., Schmitt, F., and Scholz, C.: Scaling invariance of crack surfaces, Journal of Geophysical Research: Solid Earth, 100, 5953–5973, 1995.

Schultz, R. A., Soliva, R., Fossen, H., Okubo, C. H., and Reeves, D. M.: Dependence of displacement–length scaling relations for fractures and deformation bands on the volumetric changes across them, Journal of Structural Geology, 30(11), 1405-1411, 2008

Snow, D. T.: Anisotropie permeability of fractured media, Water Resources Research, 5, 1273–1289, 1969.

Torbert, Shane. Applied computer science. Springer, 2016.

Witherspoon, P. A., Wang, J. S., Iwai, K., and Gale, J. E.: Validity of cubic law for fluid flow in a deformable rock fracture, Water resources research, 16, 1016–1024, 1980.

Zimmerman, R. W. and Bodvarsson, G. S.: Hydraulic conductivity of rock fractures, Transport in porous media, 23, 1–30, 1996.

Zimmerman, R. W. and Main, I.: Hydromechanical behavior of fractured rocks, International Geophysics Series., 89, 363–422, 2004.